
Computational Study of Magnetic Switching Mechanism of Nanoscale MRAM Cells

*Swapnil Barman**

Department of Computer Science and Engineering, Amity University, Kolkata 700135

Email: slbn99@gmail.com

Abstract

Investigation of magnetic switching of nanoscale single MRAM cells of different shapes and sizes is imperative for their applications in future magnetic memory devices. To this end, we have investigated the magnetic switching mechanism of nanoscale single MRAM cells of two different shapes with varying lateral aspect ratios by computational micromagnetic simulation. We have analysed how various parameters such as the coercive field, remanence and saturation field were affected by the variation in magnetic field. We have also analysed the change in shape of the hysteresis loops of the various samples. The magnetization reversal states were simulated to justify the spatial coherence of magnetization switching. As a result, the cells with higher aspect ratio show the Py and Fe layers forming antiparallel states in the plateau similar to synthetic antiferromagnets. As we reduce the aspect ratio, more complex quasi-uniform magnetic states are observed which are even more complicated for elliptical cells. The rectangular cell with the highest aspect ratio of 2.5 shows the most coherent and predictable switching behaviour, showing its suitability for the application of MRAM cells.

1. Introduction

The charge-based electronics is facing huge problems in miniaturization due to the fact that it is based on transistors. In current microelectronic devices the commonly used memories are dynamic random-access memory (DRAM), static RAM (SRAM), and flash memory. All of these are capacitive technologies which store data as a charge state. Over the years these memory cells have been efficiently scaled down to obtain higher speed and elevated density of memory chips in cost-effective manner [1]. However, memories based on charge storage are gradually approaching the physical limits of scalability. The emergence of zero capacitance memory (ZRAM) [2], advanced RAM (ARAM), zero impact ionization memory (Z²RAM) have provided impetus in the charge-based memory devices. However, the next step in the evolution of memory involves the design and development of universal memory. Future universal memory is expected to combine the high density of DRAM, non-volatility of flash memory and high speed of SRAM. Therefore, development of new concepts of memories based on a different storage principle will be important.

Resistive memories such as resistive random-access memory (RRAM) and magnetoresistive random access memory (MRAM) hold great promises as an alternative to charge based RAM. MRAM is one of the success stories of the rapidly emerging field of magnetoelectronics or spintronics, which uses the spin degree of freedom of electron in addition to the charge degree of freedom [3]. Unlike in charge-based RAM, in MRAM data is not stored as electric charge or current, but by magnetic elements. The elements consist of two ferromagnetic thin layers, each of which can possess a magnetization, which are separated by a thin insulating layer. The magnetic state of one of those two ferromagnetic layers is set along a particular direction (reference layer: RL) while keeping the magnetization of the other layer freely changing (free layer: FL) by an external field to store memory. The FL can be switched between the two magnetic states, namely parallel and anti-parallel to the fixed magnetization direction of the RL. The antiparallel and parallel states exhibit different magnetoresistance values which are mapped to '0' and '1' of the binary memory state. This device is known as a magnetic tunnel junction (MTJ) [4], which is the simplest unit for an MRAM bit. A memory device is built from a network of such memory cells.

The two most important magnetoresistance phenomena are known as the giant magnetoresistance (GMR) and the tunnel magnetoresistance (TMR) effect. TMR was discovered in 1975 by Julliere in a Fe/Ge/Co junction at low temperature ($T \leq 4.2\text{K}$) [5]. It was detected in a pillar composed of two ferromagnetic layers separated by a thin insulating layer, i.e. an MTJ. The resistance of the pillar depends on the magnetization direction of layers with respect to each other and is expressed as:

$$TMR = \frac{R_{AP} - R_P}{R_P} \quad [1]$$

where, R_{AP} and R_P correspond to the resistance in antiparallel (high resistance) and parallel (low resistance) magnetic states. This can be interpreted as follow. The electrons with specific spin orientation ('spin-up' or 'spin-down') can tunnel from one ferromagnetic layer into another through a non-conducting thin insulating barrier layer, if free states with the same spin orientation are available. In case of the parallel state, the majority spin ('spin-up') and minority spin ('spin-down') electrons can easily tunnel through the barrier to the other ferromagnetic layer and fill the majority ('up') and minority ('down') states, resulting in a low resistive state. On the contrary, in the antiparallel state, the majority spin ('spin-down') and minority spin ('spin-up') electrons from first ferromagnetic layer will fill the minority ('down') and majority ('up') states in the second ferromagnetic layer, respectively, leading to a low conductance, i.e. a high resistive state. On the other hand, GMR occurs in typical spin valve system consisting of two thin ferromagnetic layers separated by a thin metallic spacer. Here, the magnetoresistance (MR) occurs due to spin-dependent scattering of the electrons at the interface depending on the parallel and antiparallel magnetic states of the two ferromagnetic layers.

Hence, magnetic switching behaviour of the magnetic layers in MRAM is of utmost importance. In conventional MRAM with cross-wire architecture the data writing and reading are done by sending electrical current through the wires (write and read lines) where the magnetic switching or reversal of the layers is achieved by the Oersted magnetic field generated by the current. With the miniaturization of the MRAM cells, the required switching field and the current become very high, leading to loss of energy by Joule heating and the ensuing thermal runaway problem. Subsequently, to solve this problem new technology in the form of spin transfer torque MRAM (STT-MRAM) has been discovered [6]. Here, the magnetization of the electrons is switched using a spin-polarized current. This effect occurs in an MTJ or a spin-valve, and the STT-MRAM devices use STT tunnel junctions (STT-MTJ). Consequently, Everspin has started producing 1GB STT-MRAM chips and IBM will use these chips for its next generation FlashCore modules [6].

Here, the magnetic switching behaviour of nanoscale MRAM cells in the form of $\text{Ni}_{80}\text{Fe}_{20}(\text{Py})/\text{Al}_2\text{O}_3/\text{Fe}$ has been studied by computational micromagnetic simulation. Two different shapes of the MRAM cells, namely rectangular and elliptical have been considered where the lateral aspect ratio (eccentricity) of the cells has been varied. A stark variation in magnetic hysteresis loops (magnetization vs. applied magnetic field) along with saturation field, coercive field, remanence as well as the switching behaviour is observed with the variation in the aspect ratio for both the shapes. We have further simulated the magnetization reversal states to understand the observed behaviour.

2. Methods

The computer simulation of the magnetic hysteresis loops (magnetization (\mathbf{M}) vs. external magnetic field (\mathbf{H}) was performed by LLG micromagnetic simulator [7]. Here, the magnetization dynamics is governed by the Landau-Lifshitz-Gilbert (LLG) equation as given below.

$$\frac{d\mathbf{M}}{dt} = -\gamma(\mathbf{M} \times \mathbf{H}_{\text{eff}}) + \frac{\alpha}{M_s} \left(\mathbf{M} \times \frac{d\mathbf{M}}{dt} \right) \quad [2]$$

Here, the first term is the magnetization precession torque under the application of a magnetic field (\mathbf{H}) while the second term is the damping torque. γ is the gyromagnetic ratio, \mathbf{M} is the magnetization vector and \mathbf{H}_{eff} is the effective magnetic field consisting of various terms as given below.

$$H_{\text{eff}} = H + H_{\text{ex}} + H_{\text{d}} + H_{\text{K}} \quad [3]$$

Here, H_{ex} is the exchange interaction field, H_d is the demagnetizing field and H_K is the anisotropy field. In case of the Py/Al₂O₃/Fe MRAM element, H_{ex} consists of the exchange energies of both the Py and the Fe layers, while the interlayer exchange A_{ij} is considered as zero in our calculation. H_d incorporates the demagnetizing fields of both the magnetic layers and it depends on the size, shape and aspect ratio of the elements and is expected to change as we vary the abovementioned factors in our simulation. H_K consists of the magnetocrystalline anisotropy of the two layers. α is the dimensionless damping coefficient and M_s is the saturation magnetization. In the simulation the LLG equation is solved using finite difference method. There the geometry of the studied MRAM elements are divided into cuboidal cells of 10 nm x 10 nm x 10 nm dimensions. The element geometry, dimensions of, the number of layers and their properties are defined using a graphical user interface (GUI) of the software. In these simulations two sample shapes have been used, namely rectangular and elliptical, where the length (L) of the elements was varied as 250, 225, 200, 150, 100 and 50 nm, while the width has been fixed at 100 nm. Consequently, the lateral aspect ratio (AR) varies as 2.5, 2.25, 2.0, 1.50, 1.0 and 0.50. The thickness of each layer is fixed at 10 nm. The material parameters used in the simulation are tabulated in Table 1. Here, A_{ex} is the exchange constant of each layer, K_{u2} is the uniaxial magnetic anisotropy constant and A_{ij} is the interlayer exchange.

| Material | M_s (emu/cm ³) | γ (MHz/Oe) | A_{ex} (μ erg/cm) | K_{u2} (erg/cm ³) | A_{ij} (μ erg/cm) |
|-----------------------------------|---------------------------------|----------------------|-----------------------------|------------------------------------|-----------------------------|
| Ni ₈₀ Fe ₂₀ | 800 | 17.600 | 1.050 | 1000.00 | 0.000 |
| Fe | 1714 | 17.600 | 2.100 | 0.00 | 0.000 |

Table 1: Simulation parameters are listed in the table for two magnetic layers.

LLG equation is an ordinary differential equation which is solved using 'Time Integration – Rotation Matrices' method with a three-dimensional (3D) complex fast Fourier transformation (FFT) method. In the simulation, time Step of 1 ps, exit criteria of Max-M and convergence of 1.000e-004 is used. Maximum iteration of 25000 with the Gilbert damping (α) of 1.0 was used for fast convergence at each step to find the equilibrium magnetization at each magnetic field step. For calculation of hysteresis loops the magnetic field (H) was ramped between up to ± 5000 Oe depending on the saturation field of the sample. The hysteresis loops averaged over the sample volume is collected for each sample. In addition, the magnetization distributions over the magnetic layers for each sample have been studied to understand the reversal modes and spatial coherence of magnetization switching.

3. Results and Discussions

3.1. Effects of Element Shape of Magnetic Switching of MRAM Cells:

The simulated magnetic hysteresis loops with magnetic field applied along x-axis and showing the magnetization switching behavior for the rectangular Py/Al₂O₃/Fe MRAM elements with varying AR is

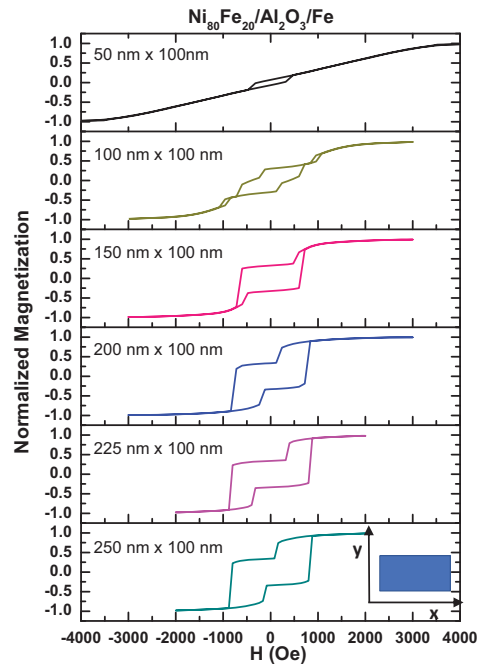


Fig. 1. Simulated magnetic hysteresis loops (normalized magnetization vs. magnetic field) for rectangular Py/Al₂O₃/Fe MRAM elements with varying AR. The maximum magnetic field was adjusted according to the saturation of magnetization for each element. The magnetic field is applied along x-axis.

shown in Fig. 1. For the elements with higher AR ($2.5 \leq AR \leq 1.5$) clear two-step switching of magnetization are observed. However, the value of the first plateau of the loop shrinks at the expense of expansion of the second plateau with the reduction of AR. The coercive field (H_c) and the remanence (M_r) also systematically decrease with the reduction of AR. On the contrary, the saturation field (H_{sat}) shows an increase with the reduction in AR. The squareness of the loops gradually decreases with the decrease in AR and become nearly hard-axis-like loop for $AR \leq 1.0$ although with some reminiscent hysteresis. This is because the elements undergo a transition from easy-axis to hard-axis of its shape anisotropy *w.r.t.* the applied field direction with the reduction of AR. For $AR = 1.0$ a three-step loop with a field-crossing is observed. For $AR = 0.5$, the loop becomes nearly hard-axis-like loop with a small hysteresis at the center of the loop. The extracted magnetic parameters (H_c , M_r and H_{sat}) are plotted in Fig. 2, which show behaviors as discussed above.

The simulated magnetic hysteresis loops with magnetic field applied along x-axis and showing the

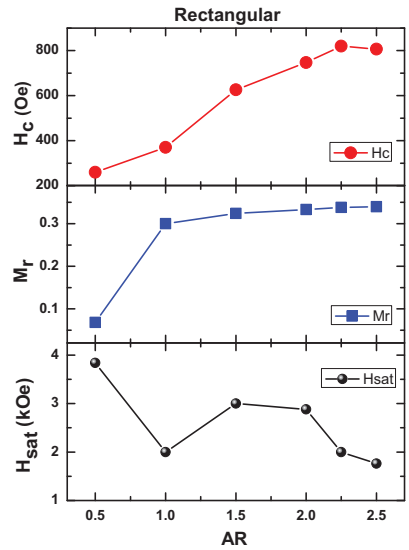


Fig. 2. Extracted magnetic parameters (H_c , M_r and H_{sat}) as a function of AR of rectangular shaped Py/ Al_2O_3 /Fe MRAM elements.

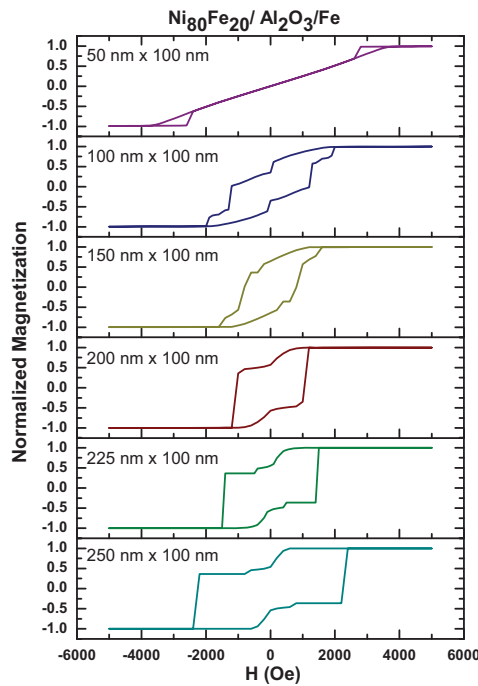


Fig. 3. Simulated magnetic hysteresis loops (normalized magnetization vs magnetic field) for elliptical Py/ Al_2O_3 /Fe MRAM elements with varying AR. The maximum magnetic field was adjusted according to the saturation of magnetization for each element. The magnetic field is applied along x-axis.

magnetization switching behaviour for the elliptical Py/ Al_2O_3 /Fe MRAM elements with varying AR is shown in Fig. 3. For the elements with higher AR ($2.5 \leq AR \leq 2.0$) two-step switching of magnetization are

observed. The values of the first and the second plateau shrink together with the reduction of AR. The coercive field (H_c) and the remanence (M_r) also systematically decrease with the reduction of the AR. The saturation field (H_{sat}) shows a decrease with the decrease in AR till two-step switching of magnetization is observed. As we reduce the AR below that, the saturation field starts to increase. The squareness of the loops gradually decreases with the decrease in AR and become a hard-axis-like loop for $AR < 1.0$ with no remanent hysteresis. The elements undergo a transition from easy-axis to hard-axis of its shape anisotropy *w.r.t.* the applied field direction with the reduction of AR. For $AR (1 \leq AR \leq 1.5)$ three-step loops are observed. For $AR = 0.5$, the loop becomes a hard-axis-like loop with one-step switching and no hysteresis at the centre of the loop. The extracted magnetic parameters (H_c , M_r and H_{sat}) are plotted in Fig. 4, which show

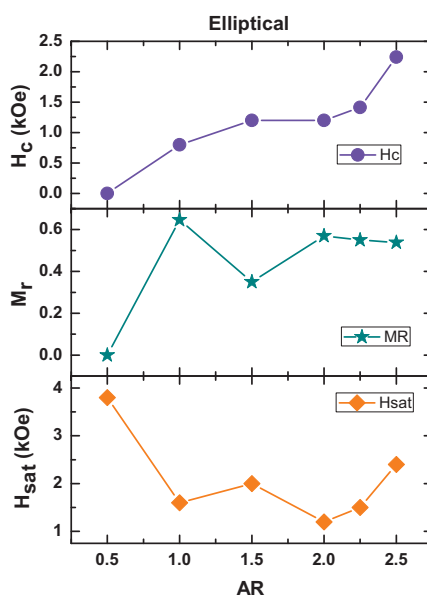


Fig. 4. Extracted magnetic parameters (H_c , M_r and H_{sat}) as a function of AR of elliptical shaped Py/ Al_2O_3 /Fe MRAM elements.

behaviour as discussed above.

3.2. Effects of Element Shape on Magnetization Reversal Modes of the MRAM Cells:

Understanding the magnetization reversal mechanism is important in nanoscale magnetism and its application in memory devices [8]. We have further simulated the magnetization distributions (maps) of two magnetic layers during the magnetization reversal (switching). In Fig. 5 we show the magnetization maps of the Py and the Fe layers at some important magnetic field values for three rectangular shaped MRAM cells with AR of 2.5, 1.0 and 0.5. The magnetization maps are placed next to the corresponding hysteresis loops where the arrows indicate the field values at which the maps are simulated. The colour map corresponding to

the magnetization direction is shown in the rightmost graph where red and blue correspond to the magnetization being aligned along the +x and -x direction, respectively, while black corresponds to magnetization being aligned along an intermediate direction. For $AR = 2.5$, in the positive saturation (1), both the Py and Fe layers align along the +x-axis, while their edge regions are slightly deviated from +x-direction. At the first plateau (2) the Py layer switches coherently, while Fe layer retains its magnetization direction. At the negative saturation (3) both the layers switch towards the negative field direction. For $AR = 1.0$, again at the positive saturation field (1) the magnetization of Py and Fe layers are aligned along the +x direction. At the first plateau (2) the Py layer partially switches its magnetization forming a quasi-uniform magnetic state (S-state), while Fe layer retains its original magnetization direction. At the second plateau (3) the Py layer almost fully switches to -x direction, while Fe switches partially forming an S-state. At the negative saturation (4) both the layers fully switch their magnetization towards -x direction. During reversal of the magnetic field, at the first plateau (5) the Py layer partially switches forming an S-state while Fe

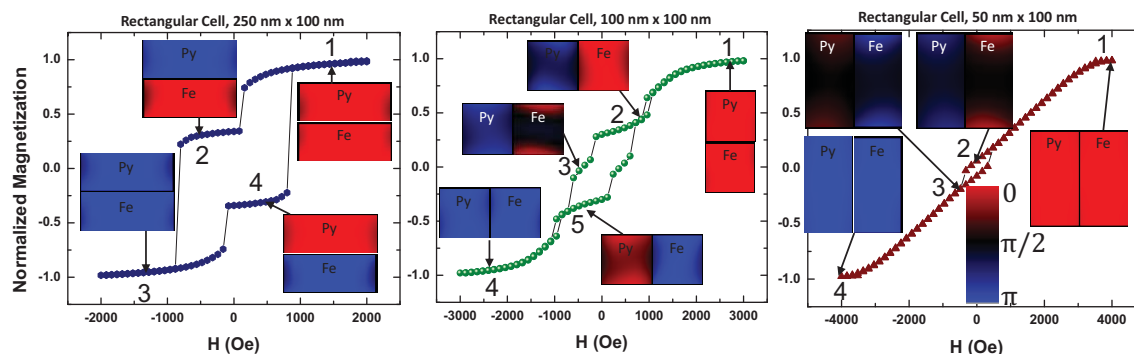


Fig. 5. Magnetization reversal states of Py and Fe layers of the MRAM cells of three different aspect ratios. The magnetic fields corresponding to which the magnetization maps are presented are marked by numbers, while the colourmap for the magnetization maps are shown in the graph for $AR = 0.5$.

retains its magnetization direction along -x direction. For $AR = 0.5$, both Py and Fe layers are fully aligned along the +x direction at the positive saturation field (1). At $H = 0$ (2) the Py layer partially switches its magnetization towards -x direction forming an S-state, while the Fe layer magnetization partially retains towards +x direction although its magnetization at the central parts starts to deviate from the +x direction forming an opposite S-state *w.r.t.* the Py layer. At $H = -480$ Oe where a minor switching in the hysteresis loop is observed (3), the Fe layer switches to -x direction but the Py layer switches back to the +x direction. This unusual observation occurs due to the fact that at this small external magnetic field the dynamics is dominated by the dipolar interaction field, the latter favours antiparallel alignment of the neighbouring magnetic layers. At the negative saturation field (4) both the layers coherently switch their magnetization to -x-direction.

In Fig. 6 we show the magnetization maps of the Py and the Fe layers at some important magnetic field values for three elliptical shaped MRAM cells with AR of 2.5, 1.0 and 0.5. For AR = 2.5, in the positive saturation (1), both the Py and Fe layers align along the x-axis. At the first step of decaying magnetization (2) the Py layer partially switches its magnetization forming a quasi-uniform magnetic state (C-state), while Fe layer retains its original magnetization direction. At the first plateau (3), the Py layer fully switches to -x direction, while Fe layer still retains its original magnetization direction. At the negative saturation (4) both the layers fully switch their magnetization towards -x direction. For AR = 1.0, again at the positive saturation field (1) the magnetization of Py and Fe layers are aligned along the +x direction. At the first step

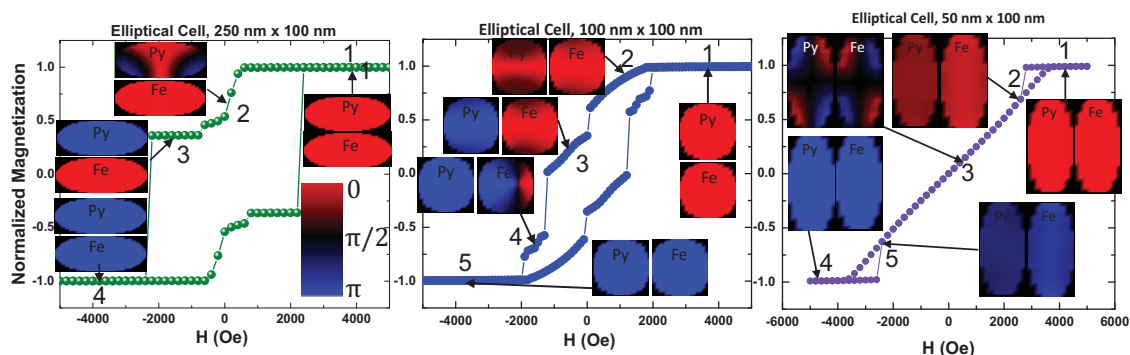


Fig. 6. Magnetization reversal states of Py and Fe layers of the MRAM cells of three different aspect ratios. The magnetic fields corresponding to which the magnetization maps are presented are marked by numbers, while the colourmap for the magnetization maps are shown in the graph for AR = 2.5.

of decaying magnetization (2) the edges of the Py layer become more demagnetized, while the edges of the Fe layer become less demagnetized. At the first plateau (3), the Py layer fully switches to -x direction, while the Fe layer becomes a little more demagnetized. At the second plateau (4), the Py layer retains its magnetization in the -x direction, while the Fe layer enters into a shifted-core vortex state [9]. At the negative saturation (5) both the layers fully switch their magnetization towards -x direction. For AR = 0.5, again at the positive saturation field (1) the magnetization of Py and Fe layers are aligned along the +x direction. Right after a minor switching (2) the Py layer starts getting demagnetized, while the edges of the Fe layer become less demagnetized. At H = 800 Oe (3), both the Py and Fe layers enter into two opposite edge domain states. At the negative saturation (4) both the layers fully switch their magnetization towards -x direction.

4. Conclusion

In summary, we have investigated the magnetic switching mechanism in nanoscale single MRAM cells of two different shapes having a varying lateral aspect ratio by using computational micromagnetic

simulations. In general, we have observed an increase in the coercive field and remanence and a decrease in the saturation field with the increase in aspect ratio of the cells. The loops have higher squareness with the characteristic two step switching for higher aspect ratio cells, which become more complicated with multi-step switching and hard-axis like curved structure with the reduced aspect ratio. The magnetization reversal states were also simulated to underpin the spatial coherence of magnetization switching. Clearly the higher aspect ratio cells show coherent spatially switching of the Py and Fe layers forming antiparallel states in the plateau similar to synthetic antiferromagnets [10]. With the reduction of aspect ratio more complex quasi-uniform magnetic states are observed which becomes even more complicated for the elliptical cells where shifted-core vortex and edge domain states appear during reversal. The rectangular cell with highest aspect ratio of 2.5 exhibits most coherent and predictable switching behaviour delineating its suitability for the application in MRAM cells. Further downscaling of this structure is feasible for increasing the areal density of MRAM devices.

5. Acknowledgements

The author gratefully acknowledges the Spintronics and Spin Dynamics Research Group of the S. N. Bose National Centre for Basic Sciences for allowing to use computational resources to carry out this work.

REFERENCES

- [1] S. Hong, Memory Technology Trend and Future Challenges, In Proceedings of the IEEE International Electron Devices Meeting (IEDM), pages 12.4.1–12.4.4, (2010).
- [2] S. Okhonin, M. Nagoga, E. Carman, R. Beffa, and E. Faraoni, New Generation of Z-RAM, In Proceedings of the IEEE International Electron Devices Meeting (IEDM), pages 925–928, (2007).
- [3] I. Zutic, J. Fabian and S. Das Sarma, Rev. Mod. Phys. 76, 323 (2004).
- [4] J. S. Moodera, Lisa R. Kinder, Terrilyn M. Wong, and R. Meservey, Large Magnetoresistance at Room Temperature in Ferromagnetic Thin Film Tunnel Junctions, Phys. Rev. Lett. 74, 3273 (1995).
- [5] M. Julliere, Tunneling Between Ferromagnetic Films. Physics Letters A, 54, 225 (1975).
- [6] MRAM-info: <https://www.mram-info.com/stt-mram>
- [7] M. R. Scheinfein and E. A. Price, 2003 *LLG User Manual* v2.50 <http://llgmicro.home.mindspring.com>.
- [8] R. Skomski, J. Phys.: Condens. Matter 15, R841 (2003).
- [9] T. Shinjo, T. Okuno, R. Hassdorf, K. Shigeto, T. Ono, Science 289, 930 (2000).
- [10] R. A. Duine, K.-J. Lee, S. S. P. Parkin, and M. D. Stiles, Nat. Phys. 14, 217 (2018).